



This is a repository copy of *Investigation of Antisite Defect Formation and Chemical Expansion in LiNiPO₄ by in Situ Neutron Diffraction*.

White Rose Research Online URL for this paper:
<http://eprints.whiterose.ac.uk/117408/>

Version: Accepted Version

Article:

Biendicho, J.J., Hsiao, K.-C., Hull, S. et al. (1 more author) (2017) Investigation of Antisite Defect Formation and Chemical Expansion in LiNiPO₄ by in Situ Neutron Diffraction. *Inorganic Chemistry*, 56 (6). pp. 3657-3662. ISSN 0020-1669

<https://doi.org/10.1021/acs.inorgchem.7b00109>

This document is the Accepted Manuscript version of a Published Work that appeared in final form in *Inorganic Chemistry*, copyright © American Chemical Society after peer review and technical editing by the publisher. To access the final edited and published work see <https://doi.org/10.1021/acs.inorgchem.7b00109>.

Reuse

Unless indicated otherwise, fulltext items are protected by copyright with all rights reserved. The copyright exception in section 29 of the Copyright, Designs and Patents Act 1988 allows the making of a single copy solely for the purpose of non-commercial research or private study within the limits of fair dealing. The publisher or other rights-holder may allow further reproduction and re-use of this version - refer to the White Rose Research Online record for this item. Where records identify the publisher as the copyright holder, users can verify any specific terms of use on the publisher's website.

Takedown

If you consider content in White Rose Research Online to be in breach of UK law, please notify us by emailing eprints@whiterose.ac.uk including the URL of the record and the reason for the withdrawal request.



eprints@whiterose.ac.uk
<https://eprints.whiterose.ac.uk/>

**Investigation of antbsite defect formation and chemical expansion in LiNiPO₄ by in situ
neutron diffraction**

Jordi Jacas Biendicho^{1*}, Kuang-Che Hsiao^{2,4}, Stephen Hull³ and Anthony R. West⁴

¹ IREC, Catalonia Institute for Energy Research, Jardins de les Dones de Negre 1, 08930, Sant Adrià de Besòs, Spain.

² Department of Product Development, SYnergy ScienTech Corp., 7F, No.9, Park Ave. II, Hsinchu Science Park, Hsinchu, Taiwan 30075.

³ The ISIS facility, STFC Rutherford Appleton Laboratory, United Kingdom

⁴ Department of Materials Science and Engineering, University of Sheffield, S1 3JD, UK

*Corresponding author: jjacas@irec.cat

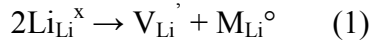
Abstract

In situ neutron diffraction has been used to characterize the effect of temperature on the crystal structure of LiNiPO₄. LiNiPO₄ adopts an ordered olivine structure at room temperature but, with increasing temperature, this work shows that a significant amount of Li and Ni cation exchange occurs, e.g. ~ 15 % at 900 °C. The antisite disorder is detected by residual nuclear densities on the M1 and M2 octahedral sites in the olivine structure using difference Fourier maps and by changes in cation site occupancies, lattice parameters and mean <M-O> bond distances. The antisite disorder is also responsible for chemical expansion of the crystal lattice in addition to thermal expansion. Antisite defect formation at high temperature and its reversibility on cooling can be understood as an entropically-driven feature of the crystal structure of LiNiPO₄. The lithium ion diffusion pathway, that follows a curved trajectory along the *b* axis in the olivine structure, is, therefore, susceptible to be blocked if synthesis conditions are not carefully controlled and should also be influenced by the chemically expanded lattice of the disordered structure if this is preserved to ambient temperature by rapid cooling.

Introduction

The mineral olivine is a magnesium iron silicate with formula $(\text{Mg,Fe})_2\text{SiO}_4$ and is generally found in mafic or ultramafic igneous rocks. The name olivine also refers to a common crystal structure adopted by many oxides with general formula M_2XO_4 , where M is a transition metal and/or alkaline earth metal and X is usually P or Si. Materials with the olivine structure can be viewed as polyanionic compounds that contain isolated tetrahedra, $(\text{XO}_4)^{n-}$ sharing edges and vertices with two non-equivalent octahedral positions, M1 and M2. This arrangement leads to an ordering of cations of different size and charge between the two octahedral sites depending on sample thermal history^{1,2}. Investigation of cation disorder in olivines as a function of temperature by *in situ* neutron diffraction has provided estimates of cooling rates which can be related to processes that occurred during cooling of the earth's mantle³. An additional view of the olivine structure is as the hexagonal close packed analogue of the cubic spinel structure, in which one half of the octahedral sites and one eighth of the tetrahedral sites are occupied by Mg, Fe and Si, respectively.

Interest in olivine-structured materials as cathodes for Li ion batteries emerged in 1997 when LiFePO_4 ⁴ was presented as an alternative cathode to LiCoO_2 ⁵ and LiMn_2O_4 ⁶. LiMPO_4 (M=Mn, Fe, Co and Ni) materials deliver a significant amount of electrochemical capacity ($\sim 165 \text{ mAhg}^{-1}$) at high voltages which are dependent on the redox-active transition metal cations⁷. Their electrochemical performance, however, depends on synthesis conditions, and the use of conductive additives⁸. Low temperature synthesis methods lead to materials that are thermodynamically metastable; defect concentrations may be high and usually take the form of sarcopside-like defects that can be represented by:



where the superscripts ' , x, and ° refer to nominal site charges of -1, 0 and +1, respectively and M refers to Mn, Fe, Co or Ni. Li-deficient materials, i.e. Li_xMPO_4 : $x < 1$, have been prepared by hydrothermal⁹⁻¹¹ or flux growth techniques¹² and for M=Fe, show significant iron disorder between M1 and M2 sites. The exact nature of the defect(s) may be difficult to elucidate. However, neutron diffraction (ND) has proven to be a powerful technique to determine the average structure of materials, particularly those in which disordered cations have a significant contrast in their neutron scattering lengths^{2,13}.

Previously, we reported significant Li-Fe site exchange in LiFePO_4 quenched from high temperature. This was detected by changes in lattice parameters and cation site occupancies by Rietveld refinement of the crystal structure using X-Ray powder diffraction (XRD data)¹⁴. The Li-Fe site exchange or antisite defect can be represented by:



The antisite defect was shown by computer simulation to be the preferred defect in the olivine structure^{15,16} and has been observed using annular dark-field scanning transmission electron microscopy (STEM) in samples prepared by solid state reaction¹⁷. Antisite defects are randomly distributed without aggregation for LiMnPO_4 but with strong clustering in LiFePO_4 ¹⁸.

The occupancy of M1 sites by M^{2+} cations in samples prepared either by low temperature synthesis or high temperature reaction is detrimental to performance as a cathode in Li ion batteries. Thus, with a high degree of cation disorder, Li atoms are blocked along the *b* axis,

leading to reduced cathode capacity¹⁹. In LiCoPO₄, capacity fading was attributed to *in situ* formation of antisite defects during battery cycling^{20,21}.

We have prepared LiNiPO₄ by solid state reaction and characterized its structure as a function of temperature by Rietveld refinement of ND data. To our knowledge, significant efforts have been made to understand the nature of defects in LiFePO₄ and LiMnPO₄ but less so for the Ni analogue. LiNiPO₄ cycles electrochemically at potentials > 5 V vs Li metal and its performance has been improved with respect to the pristine form by carbon coating and other approaches²²⁻²⁵. However, Li-ion batteries with LiNiPO₄ as cathode are still far from optimised due to problems with electrolyte stability²⁶. In this paper, we demonstrate that a significant concentration of antisite defects forms in LiNiPO₄ as a function of temperature leading to chemical expansion of the olivine structure.

Experimental

LiNiPO₄ was synthesized from stoichiometric amounts of Li₂CO₃ (Aldrich, 99%), NiCO₃ (Alfa Aesar, 99%) and (NH₄)H₂PO₄ (Fluka, ≥99%) by conventional solid-state reaction. Samples were mixed by ball milling using zirconia beads as milling media with isopropanol at a constant speed of 30 rpm for 24 h. The mixtures were precalcined at 120°C for 12 h and then heated in air at 500°C for 4 h to drive off H₂O and CO₂, respectively. The decomposed powders were reground and heated at 800°C for 48 h in air. The final product was cooled slowly to room temperature (RT).

Phase purity was determined by a high-resolution STOE STADI P X-ray diffractometer (STOE & Cie GmbH, Germany) operated at 40 kV and 35 mA with Cu K_{α1} (1.5406 Å) radiation in transmission mode using a position sensitive detector (PSD). The scanning step size and counting time were set at 0.2° and 100 seconds in the 2θ range 10–100°.

ND data as a function of temperature were collected using the Polaris powder diffractometer²⁷ at the ISIS neutron spallation source. The use of neutrons to characterize LiNiPO₄ is advantageous over synchrotron radiation since ND allows determination of the location and occupancy of light elements such as Li in the presence of heavier ones such as Ni. Table 1 shows ionic radii²⁸ and neutron scattering lengths²⁹ of the elements in LiNiPO₄.

Time-of-flight ND data were collected at RT, 600, 700, 800, 850, 900, 925 and 950°C for periods of 1h after temperature stabilization and at several temperatures on subsequent cooling to check reversibility. Neutron data were first corrected for sample absorption using OpenGENIE³⁰ and then used for crystal structure refinement using GSAS³¹. The

diffraction peak shape was refined using a pseudo-Voigt function with two back-to-back exponentials and the background fitted using the Shifted Chebyshev function in GSAS³¹.

In order to obtain the best fit to the ND data, structural models involved refinement of lattice parameters, atomic positions, occupancies and thermal displacement parameters. Structural constraints were added when necessary, e.g. to evaluate Li-Ni site exchange. Residual nuclear densities not considered by the structural model(s) were investigated using a combination of FORPLOT and FORSRH routines within the GSAS software. MCE software³² was used to generate 3D Fourier maps.

Results and discussion

LiNiPO₄ synthesized by solid state reaction was investigated by XRD to check sample purity, see figure S1 in the supporting information (SI). The XRD pattern shows sharp diffraction peaks that were indexed using an orthorhombic unit cell and lattice parameters $a = 10.0334(2) \text{ \AA}$, $b = 5.8566(1) \text{ \AA}$, $c = 4.6793(7) \text{ \AA}$, $V = 274.96(6) \text{ \AA}^3$, in good agreement with those reported for samples prepared using similar synthesis methods^{25,33}. The sample was phase-pure from XRD analysis and was used for Rietveld refinement of ND data as a function of temperature.

Diffraction patterns collected between RT and 900 °C were refined using an orthorhombic unit cell with space group *Pnma* (No 62). However, data sets collected at $\geq 925 \text{ }^\circ\text{C}$, showed new reflections whose intensities were not reversible on cooling, indicating that LiNiPO₄ started to decompose during *in situ* ND measurements. Search and Match of the unknown diffraction peaks afforded two phases, Ni₂P and Li₄P₂O₇, which were added to refinements when necessary, but their crystal structures were not refined.

Figure 1a shows a model of the LiNiPO₄ unit cell in which Li (yellow spheres) and Ni (red spheres) are located on the M1 and M2 octahedral sites, respectively. P atoms are coordinated by four oxygens (blue spheres) forming tetrahedra which share edges and vertices with metal octahedra. The structure was first refined without allowing Li and Ni to exchange sites. The refinements were not fully satisfactory as shown by the difference profiles (not shown) and relatively high χ^2 , wRp and Rp values of e.g. 5.86, 6.61 %, 8.81 % for the 900 °C data set. Residual nuclear densities were evaluated by generating 3D difference Fourier density (DELF) maps, as shown in Figure 1b at 900 °C with contours at nuclear densities of + 0.20 (red) and at - 0.20 (yellow). Positive density is located along the

b axis in the form of globular contours around the M1 position whereas negative density contours are located around the M2 position. The negative residual nuclear density, observed in all data sets measured ≥ 700 °C and its associated crystallographic position, M2, was confirmed by FORSRH and is attributed to some Li atoms located in the M2 position, table 1; occupancy constraints were therefore lifted to allow exchange of Li and Ni between M1 and M2 positions at high temperatures.

Figures 2a and b show refined ND patterns at RT and 900 °C using this cation-disordered structural model. Good agreement between the structural model and neutron data is shown by the difference profile and values of the statistical parameters, Figure 2 and Tables S1-S13.

Cation disorder as a function of temperature is shown in figure 3a. Li primarily occupies the larger octahedral M1 site and Ni the M2 site, in accordance with standard ionic radius values, table 1. At higher temperatures, Li and Ni site exchange leads to significant amounts of disorder, e.g. ~ 9 and 15 % at 800 and 900 °C, respectively. The disorder is fully reversible on cooling; for example, neutron data sets at 700°C on heating and cooling show a similar refined Li occupancy on the M2 site of ~ 3 %.

Cation disorder may be understood thermodynamically in terms of:

$$\Delta G = \Delta H - T\Delta S \quad (3)$$

At high temperatures, the contribution of the $-T\Delta S$ entropy term becomes increasingly important to the free energy of the sample, ΔG , leading to significant amounts of cation disorder. Such thermally-induced disorder is a common, entropically-driven feature of the crystal structures of many minerals and compounds³⁴.

The disorder is also observed as an anomalous change in the *a* and *b* lattice parameters, figures 3b, c, and on mean <M2-O> bond distances, figure 3d. In these three cases, linear regression shows that straight lines cannot be used to fit the data adequately because the various parameters start to increase more rapidly above ~ 600 °C. The exception to this non-linear behaviour is the *c* lattice parameter and the “<M1-O>” bond distances which do show a linear dependence on temperature, figure 4a and figure 3d, respectively.

The explanation for the non-linear behaviour of some parameters is that, in addition to the usual effects of thermal expansion, an extra contribution associated with chemical expansion is present which is associated explicitly with Li, Ni cation disorder. The key parameter appears to be the mean <M2-O> bond distance which is affected greatly by the substitution of large Li⁺ for smaller Ni²⁺ whereas the opposite substitution has little extra effect on the “<M1-O>” bond distance. These structural distortions are in accordance with a structural model in which cation disorder occurs between M1 and M2 octahedra that share a common edge within the *ab* plane of the olivine structure; since “<M2-O>” shows an anomalous expansion, this is reflected in the anomalous expansion of the *a* and *b* parameters. The *c* parameter, however, appears to be controlled by “<M1-O>” and the size of the larger cation, Li and the expansion of *c* is limited to the effect of thermal expansion alone. The mean <P-O> bond distance as a function of temperature, figure 4b, shows no temperature dependence between RT and 900°C.

The ionic diffusion pathway has been characterized previously in LiFePO₄³⁵ and takes the form of a curved trajectory in the olivine unit cell. Li atoms jump between neighbouring M1 positions through one of the faces of the octahedra along *b*. The same conduction pathway is confirmed for LiNiPO₄ by Rietveld refinement of anisotropic displacement

parameters of Li atoms at 700°C. Figure 5 shows a ‘ball and stick’ model of the Li conduction pathway; refined displacement parameters for lithium atoms are shown as blue ellipsoids.

Conductivity measurements as a function of temperature for LiMPO₄ ceramics³⁶ indicate that LiNiPO₄ shows the lowest ionic conductivity compared to the Mn, Fe and Co-analogues. This is in accordance with the lowest mobility of ionic species in LiNiPO₄ due to its smallest unit cell volume e.g. 274.90(1) and 291.25 Å³ for LiNiPO₄ and LiFePO₄¹⁴, respectively. The mobility term is included using the conductivity equation (3) and is mainly controlled by the activation energy³⁴.

$$\sigma = n e \mu \quad (3)$$

where n is the number of charge-carriers, e their charge and μ their mobility.

For samples in which a large concentration of antisite defects is present, prepared either by low temperature or conventional synthesis methods, the concentration of charge-carriers taking part in n in equation 3 would be lower due to the blockage of the conduction pathway. It appears, therefore, that synthesis conditions need to be more carefully controlled in LiNiPO₄ than in other LiMPO₄ materials to maximize both ionic conductivity and electrochemical capacity of the samples since *in situ* neutron diffraction results presented in this paper have shown that the crystal structure of LiNiPO₄ can accommodate a larger concentration of antisite defects than previously reported on LiMnPO₄³⁷, LiFePO₄^{14,17} or LiCoPO₄^{20,21}.

Conclusions

Neutron diffraction measurements show that the crystal structure of LiNiPO_4 accommodates a large concentration of antisite defects at high temperature. The antisite defect is visualized on residual nuclear density maps and detected by changes in lattice parameters, cation site occupancies and mean $\langle \text{M2-O} \rangle$ bond distances. At $900\text{ }^\circ\text{C}$, $\sim 15\%$ of Li atoms are located on the M2 site. The antisite disorder is reversible on cooling, indicating that it is an entropically-driven feature of the crystal structure.

Refinement of thermal displacement parameters at high temperature indicate that Li atoms diffuse along b following a curved trajectory as reported in LiFePO_4 . It appears that the 1D conduction pathway is more likely to be blocked at high temperature in the case of LiNiPO_4 than in other LiMPO_4 materials due to the larger amount of intrinsic defects in the Ni analogue. The antisite disorder is reversible at the slow cooling rates used in the in situ neutron diffraction experiment, but the rate of equilibration on cooling is not known and some disorder may be preserved in rapidly cooled samples. Care is therefore required in the conditions used for sample synthesis, especially the cooling rate, as residual antisite disorder may influence the subsequent electrochemical behaviour.

The antisite disorder leads to an anomalous expansion of the structure at high temperatures which involves a chemical expansion in addition to the usual effect of thermal expansion.

Caption for Figures

Figure 1 a) Model of LiNiPO_4 unit cell in which lithium is shown as yellow spheres, nickel as red spheres and oxygen atoms as blue spheres b) 3D DELF map of LiNiPO_4 ; red contours show positive nuclear density and yellow contours negative density not considered by the ordered structural model.

Figure 2 Refined neutron diffraction patterns of LiNiPO_4 at a) RT and b) $900\text{ }^\circ\text{C}$ using a structural model in which Li and Ni were allowed to exchange their positions.

Figure 3 Rietveld refinement results of LiNiPO_4 as a function of temperature a) lithium occupancy in the octahedral M2 site b) a lattice parameter c) b lattice parameter and d) mean $\langle\text{M1-O}\rangle$ and $\langle\text{M2-O}\rangle$ bond distances.

Figure 4 Rietveld refinement results of LiNiPO_4 as a function of temperature a) c lattice parameter and b) mean $\langle\text{T-O}\rangle$ bond distances.

Figure 5 Ball and stick model showing the lithium conduction pathway in LiNiPO_4 extrapolated from refined anisotropic thermal parameters of lithium ions using *in situ* neutron data measured at $700\text{ }^\circ\text{C}$, shown as blue ellipsoids.

Supporting Information Available: Powder XRD of as-prepared LiNiPO_4 and Rietveld refinement results of LiNiPO_4 crystal structure for neutron diffraction patterns measured at RT, 600, 700, 800, 850, 900, 925, 950 °C and on cooling.

References

- [1] Redfern, S.A.T. Time-temperature-dependent M-site ordering in olivines from high-temperature neutron time-of-flight diffraction, *Phys. B.* **1998**, 241-243, 1189-1196.
- [2] Redfern, S.A.T.; Henderson, C.M.B.; Knight, K.S.; Wood, B.J. High-temperature order-disorder in $(\text{Fe}_{0.5}\text{Mn}_{0.5})_2\text{SiO}_4$ and $(\text{Mg}_{0.5}\text{Mn}_{0.5})_2\text{SiO}_4$ olivines: an in situ neutron diffraction study, *Eur. J. Mineral.* **1997**, 9, 2, 287-300.
- [3] Redfern, S.A.T.; Henderson, C.M.B.; Wood, B.J.; Harrison, R.J.; Knight, K.S. Determination of olivine cooling rates from metal-cation ordering, *Nature*, **1996**, 381, 407-409.
- [4] Padhi, A.K.; Nanjundaswamy, K.S.; Goodenough, J.B. Phospho-olivines as positive-electrode materials for rechargeable lithium batteries, *J. Electrochem. Soc.* **1997**, 144, 1188.
- [5] Mizushima, M.; P.C. Jones, P.C.; Wiseman, P.J.; Goodenough, J.B. Li_xCoO_2 ($0 < x \leq 1$): A new cathode material for batteries of high energy density, *Mat. Res. Bull.* **1980**, 15, 6, 783-789.
- [6] Tarascon, J.M.; Wang, E.; Shokoohi, F.K.; McKinnon, W.R.; Colson, S. The spinel phase of LiMn_2O_4 as cathode in secondary lithium cells, *J. Electrochem. Soc.* **1991**, 138, 10, 2859-2864
- [7] Zhou, F.; Cococcioni, M.; Kang, K.; Ceder, G. The Li intercalation potential of LiMPO_4 and LiMSiO_4 olivines with $M = \text{Fe, Mn, Co, Ni}$, *Electrochem. Commun.* **2004**, 6, 1144-1148.

- [8] Wang, J.; Sun, X. Understanding and recent development of carbon coating on LiFePO_4 cathode materials for lithium-ion batteries, *Energy Environ. Sci.* **2012**, 5, 5163.
- [9] Chen, J.; Vacchio, M.J.; Wang, S.; Chernova, N.; Zavalij, P.Z.; Whittingham, M.S. The hydrothermal synthesis and characterization of olivines and related compounds for electrochemical applications, *Solid State Ionics*, **2008**, 178, 1676-1693.
- [10] Paolella, A.; Bertoni, G.; Hovington, P.; Feng, Z.; Flacau, R.; Prato, M.; Colombo, M.; Marras, S.; Manna, L.; Turner, S.; Tendeloo, G.V.; Guerfi, A.; Demopoulos, G.P.; Zaghbi, K. Cation Exchange mediated elimination of the Fe-antisites in the hydrothermal synthesis of LiFePO_4 , *Nano Energy*, **2015**, 16, 256-267.
- [11] Jensen, K.M.Ø.; Christensen, M.; Gunnlaugsson, H.P.; Lock, N.; Bojesen, E.D.; Proffen, T.; Iversen, B.B. Defects in hydrothermally synthesized LiFePO_4 and $\text{LiFe}_{1-x}\text{Mn}_x\text{PO}_4$ cathode materials, *Chem. Mater.* **2013**, 25, 2282-2290.
- [12] Janssen, Y.; D. Santhanagopalan, D.; Qian, D.; Chi, M.; Wang, X.; Hoffmann, C.; Meng, Y.S.; Khalifah, P.G. Reciprocal salt flux growth of LiFePO_4 single crystals with controlled defect concentrations, *Chem. Mater.* **2013**, 25, 4574-4584.
- [13] Gibot, P.; Casas-Cabanes, M.; Laffont, L.; Levasseur, S.; Carlach, P.; Hamelet, S.; Tarascon, J.-M.; Masquelier, C. Room-temperature single-phase Li insertion/extraction in nanoscale Li_xFePO_4 , *Nature Materials*, **2008**, 7, 741-747.
- [14] Biendicho, J.J.; West, A.R. Thermally-induced cation disorder in LiFePO_4 , *Solid State Ionics*, **2011**, 203, 33-36.

- [15] Fisher, C.A.J.; Prieto, V.M.H.; Islam, M.S. Atomic-scale investigation of defects, dopants, and lithium transport in the LiFePO_4 olivine-type battery material, *Chem. Mater.* **2008**, *20*, 5907-5915.
- [16] Chung, S.-Y.; Choi, S.-Y.; Lee, S.; Ikuhara, Y. Distinct configurations of antisite defects in ordered metal phosphates: comparison between LiMnPO_4 and LiFePO_4 , *Phys. Rev. Lett.* **2012**, *108*, 195501.
- [17] Chung, S.-Y.; Choi, S.-Y.; Yamamoto, T.; Ikuhara, Y. Atomic-scale visualization of antisite defects in LiFePO_4 , *Phys. Rev. Lett.* **2008**, *100*, 125502.
- [18] Chung, S.-Y.; Choi, S.-Y.; Kim, T.-H.; Lee, S. Surface-orientation-dependent distribution of subsurface cation-exchange defects in olivine-phosphate nanocrystals, *ACS nano*, **2015**, *9*, 1, 850-859.
- [19] Chen, J.; Whittingham, M.S. Hydrothermal synthesis of lithium iron phosphate *Electrochem. Comm.* **2006**, *8*, 855-858.
- [20] Boulineau, A.; Gutel, T. Revealing electrochemically induced antisite defects in LiCoPO_4 : evolution upon cycling, *Chem. Mater.* **2015**, *27*, 802-807.
- [21] Truong, Q.D.; Devaraju, M.K.; Sasaki, Y.; Hyodo, H.; Tomai, T.; Honma, I. Relocation of cobalt ions in electrochemically delithiated LiCoPO_4 cathode materials, *Chem. Mater.* **2014**, *26*, 2770-2773.
- [22] Örnek, A.; Kazancioglu, M.Z. A novel and effective strategy for producing core-shell LiNiPO_4/C cathode material for excellent electrochemical stability using a long-time and low-level microwave approach, *Scr. Mater.* **2016**, *122*, 45-49.

- [23] Kumar, P.R.; Madhusudhanrao, V.; Nageswararao, B.; Venkateswarlu, M.; N. Satyanarayana, N. Enhanced electrochemical performance of carbon-coated LiMPO_4 (M=Co and Ni) nanoparticles as cathodes for high-voltage lithium-ion battery, *J. Solid State Electrochem.* **2016**, 20, 1855-1863.
- [24] Vijayan, L.; Cheruku, R.; Govindaraj, G. Electrical, optical and magnetic investigations on LiNiPO_4 based olivines synthesized by solution combustion technique, *Mater. Research Bull.* **2014**, 50, 341-347.
- [25] Ramana, C.V.; Ait-Salah, A.; Utsunomiya, S.; Becker, U.; Mauger, A.; Gendron, F.; Julien, C.M. Structural and characteristics of lithium nickel phosphate studied using analytical microscopy and raman spectroscopy, *Chem. Mater.* **2006**, 18, 3788-3794.
- [26] Takaya, S.; Tatsuya, M.; Marukane, S.; Takagi, K.; Ionic liquids containing carbonate solvent as electrolytes for lithium ion cells, *J. Power Sources*, **2004**, 138, 1-2, 253-261.
- [27] Hull, S.; Smith, R.I.; David, W.I.F.; Hannon, A.C.; Mayers, J.; Cywinski, R. The Polaris powder diffractometer at ISIS, *Phy. B*, **1992**, 180-181, 1000-1002.
- [28] Shannon, R.D. Revised effective ionic radii and systematic studies of interatomic distances in halides and chalcogenides, *Acta Crystallogr. Sec. A*, **1976**, 32, 751-767.
- [29] Sears, V.F. Neutron scattering lengths and cross sections, *Neutron News*, **1992**, 3, 26-37
- [30] OpenGENIE 2.3; www.open genie.org
- [31] Larson, A.C.; Von Dreele, R.B. Report LA-UR-86-748, Los Alamos National Laboratory, **1990**, NM87545.

[32] Rohlicek, J.; Husak, M. MCE2005 - A new version of a program for fast interactive visualization of electron and similar density maps optimized for small molecules, *J. Appl. Crystallogr.* **2007**, 40, 600.

[33] Inorganic Crystal Structure Database (ICSD); www.cds.dl.ac.uk

[34] West, A.R. *Solid state chemistry and its applications*, John Wiley and Sons Ltd., United Kingdom, 2014.

[35] Nishimura, S.-I.; Kobayashi, G.; Ohoyama, K.; Kanno, R.; Yashima, M.; Yamada, A. Experimental Visualization of lithium diffusion in Li_xFePO_4 , *Nat. Mat.* **2008**, 7, 707-711.

[36] Rissouli, K.; Benkhouja, K.; Ramos-Barrado, J.R.; Julien C. Electrical conductivity in lithium orthophosphates, *Mat. Sci. Eng.* **2003**, B98, 185-189.

[37] Fang, H.; Pan, Z.; Li, L.; Yang, Y.; Yan, G.; Li, G.; Wei, S.; The possibility of manganese disorder in LiMnPO_4 and its effect on the electrochemical activity, *Electrochem. Commun.* **2008**, 10, 1071-1073.

Tables

Element	Oxidation state	Ionic radii	Scattering length (b)
Li	+1	0.76	-1.90 fm
Ni	+2	0.69	10.3 fm
P	+5	0.17	5.13 fm
O	-2	1.42	5.80 fm

Table 1 Ionic radii and neutron scattering lengths of the chemical elements in LiNiPO_4

Figures

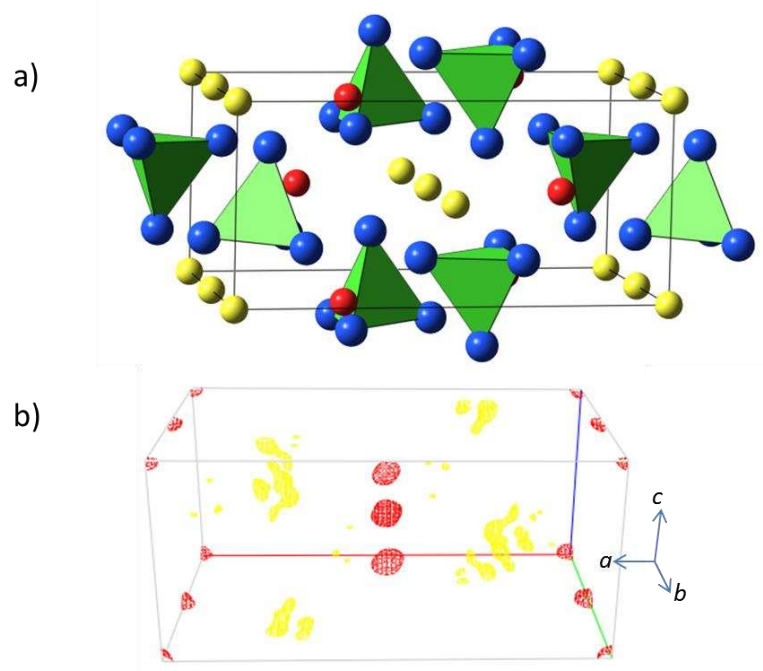


Figure 1

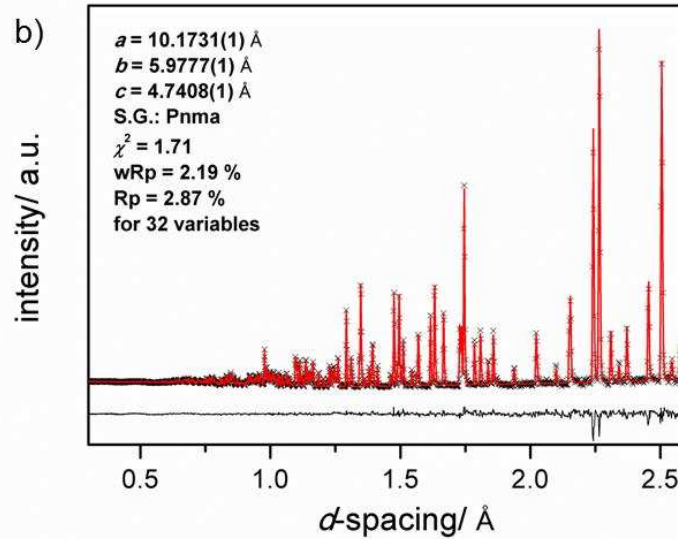
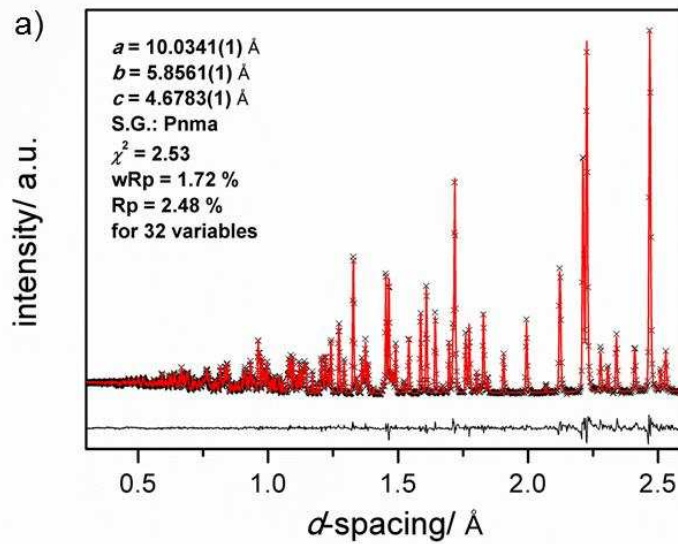


Figure 2

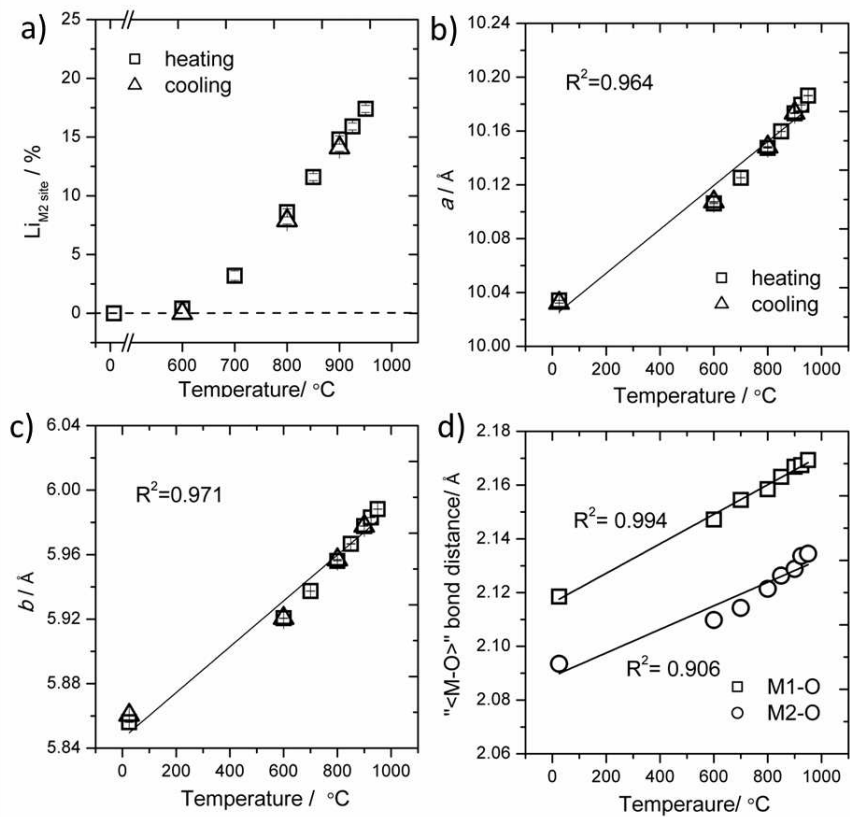


Figure 3

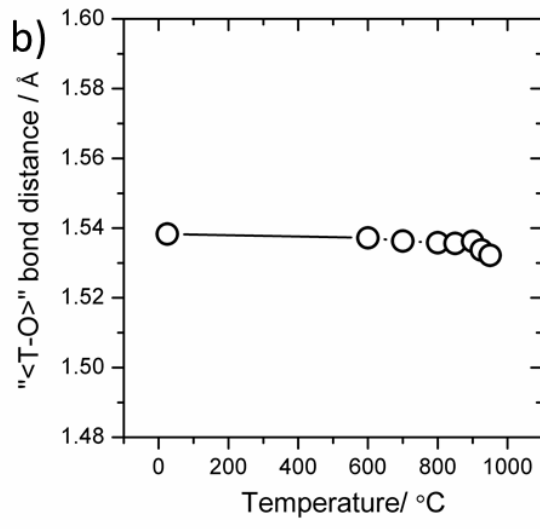
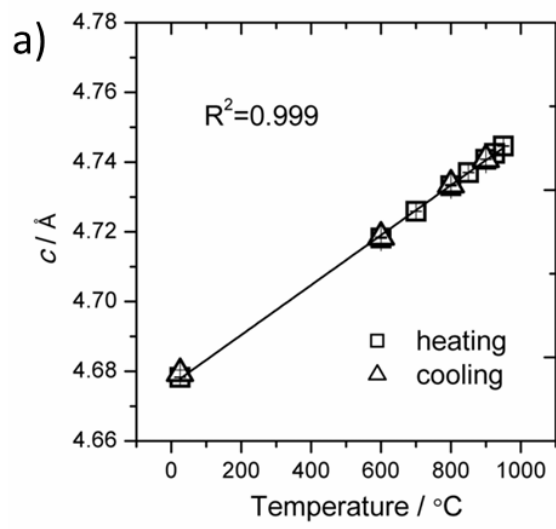


Figure 4

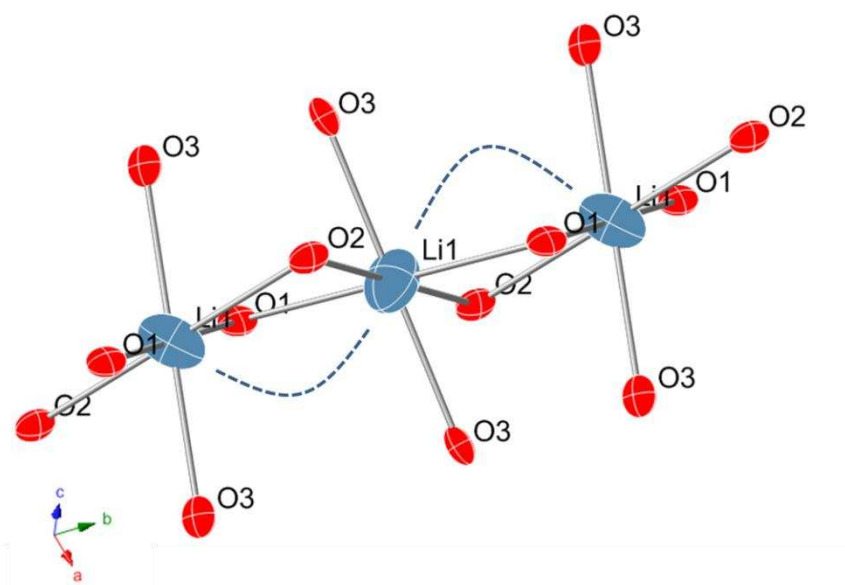


Figure 5

Table of contents Only

LiNiPO_4 adopts an ordered crystal structure at room temperature but on heating, *in situ* neutron diffraction shows that Li and Ni exchange their crystallographic positions leading to a disordered olivine structure. *In situ* diffraction studies, specially using neutron radiation due to the presence of lithium, are interesting in order to understand antisite defect formation in olivine materials and, in turn, optimise their electrochemical performance as cathode for Li ion batteries.

